THE JOURNAL OF PHYSICAL CHEMISTRY A

ARTICLE

pubs.acs.org/JPCA

Thermal Decomposition of Methyl 2-Azidopropionate Studied by UV Photoelectron Spectroscopy and Matrix Isolation IR Spectroscopy: Heterocyclic Intermediate vs Imine Formation

R. M. Pinto,*[,†] A. A. Dias,[†] M. L. Costa,[†] P. Rodrigues,[‡] M. T. Barros,[§] J. S. Ogden,[∥,⊥] and J. M. Dyke[∥]

[†]CFA, Departamento de Física, Faculdade de Ciências e Tecnologia, FCT, Universidade Nova de Lisboa, 2829-516 Caparica, Portugal

[‡]ITQB, Instituto de Tecnologia Química e Biológica, Universidade Nova de Lisboa, 2780-901 Oeiras, Portugal

[§]REQUIMTE, Departamento de Química, Faculdade de Ciências e Tecnologia, FCT, Universidade Nova de Lisboa, 2829-516 Caparica, Portugal

[∥]Department of Chemistry, The University of Southampton, Southampton SO17 1BJ, U.K.

Supporting Information

ABSTRACT: Methyl 2-azidopropionate ($N_3CH_3CHCOOCH_3$, M2AP) has been synthesized and characterized by different spectroscopic methods, and the thermal decomposition of this molecule has been investigated by matrix isolation infrared (IR) spectroscopy and ultraviolet photoelectron spectroscopy (UVPES). Computational methods have been employed in the spectral simulation of both UVPES and matrix IR spectra and in the rationalization of the thermal decomposition results. M2AP presents a HOMO vertical ionization energy (VIE) of 9.60 ± 0.03 eV and contributions from all four lowest-energy conformations of this molecule are detected in the gas phase. Its thermal decomposition starts at ca. 400 °C and is complete at ca. 650 °C, yielding N_2, CO, CO_2, CH_3CN, and CH_3OH as the final decomposition products. Methyl formate (MF) and CH_4 are also found during the pyrolysis process. Analysis of the potential energy surface of the decomposition of M2AP indicates that M2AP decomposes preferentially into the corresponding imine (M2IP), through a 1,2-H shift synchronous with the N_2 elimination (Type 1 mechanism), requiring an activation energy of 160.8 kJ/mol. The imine further decomposes via two competitive routes: one accounting for CO, CH_3OH, and CH_3CN (ΔE_{G3} = 260.2 kJ/mol) and another leading to CO_2, CH_4, and CH_3CN (ΔE_{G3} = 268.6 kJ/mol). A heterocyclic intermediate (Type 2 mechanism)—4-Me-5-oxazolidone—can also be formed from M2AP via H transfer from the remote O−CH_3 group, together with the N_2 elimination (ΔE_{G3} = 260.2 kJ/mol). Finally, a third pathway which accounts for the formation of MF through an M2AP isomer is envisioned.

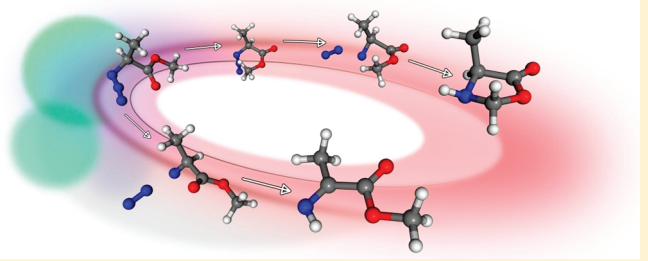

1. INTRODUCTION

The gas-phase thermal decomposition of azides (R−N_3) has long been an exciting and interesting research subject,[1] mainly due to the fact that these molecules release nitrogen very easily, together with a high amount of energy, when heated. Therefore, most practical applications of azides are based on this property, whether being adopted as building blocks in organic chemistry synthesis[2] or being used as energetic additives for solid propellants.[3] Their uses span a wide range of areas, from industrial to pharmaceutical and biological applications.

An important element in the study of the thermal decomposition of azides is the potential for detecting reactive, often unstable, intermediate compounds. Some successful examples are the cases of methanimine[4,5] (H_2C=NH), 2-iminoacetamide[6] ($H_2NCOCHNH$), iminodimethyl acetamide,[7] and 2-oxazolidone[7] ($C_3H_5NO_2$).

The extensive studies undertaken by Dyke and co-workers on the thermal decomposition of organic azides,[6,7] using UV photoelectron spectroscopy (UVPES) and the matrix isolation IR technique, have led to the establishment of two main decomposition mechanisms.

The Type 1 mechanism (see Scheme 1), originally proposed by Bock,[4] involves the loss of N_2 and formation of the imine associated with the parent azide. Within a Type 1 mechanism, a 1,2-H shift always occurs, the question being if it starts after or before the N_2 loss. In the first case, a singlet nitrene is left from the N_2 elimination, and then it converts into a more stable imine, through a 1,2-H shift. In the second case, the 1,2-H shift itself promotes the dissociation of N_2 and leads to the formation of the imine, in a synchronous way. The Type 1 mechanism was successfully proposed to explain the thermal decomposition of 2-azidoethanol[8] ($N_3CH_2CH_2OH$), 2-azidoacetamide[6] ($N_3CH_2CONH_2$), and 2-azido-*N*,*N*-dimethylacetamide[7] ($N_3CH_2CONMe_2$).

Received: April 20, 2011
Revised: June 24, 2011
Published: June 27, 2011

Scheme 1

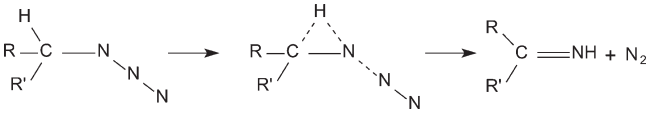

Scheme 2

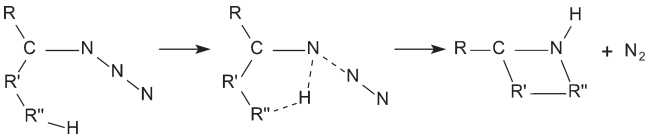

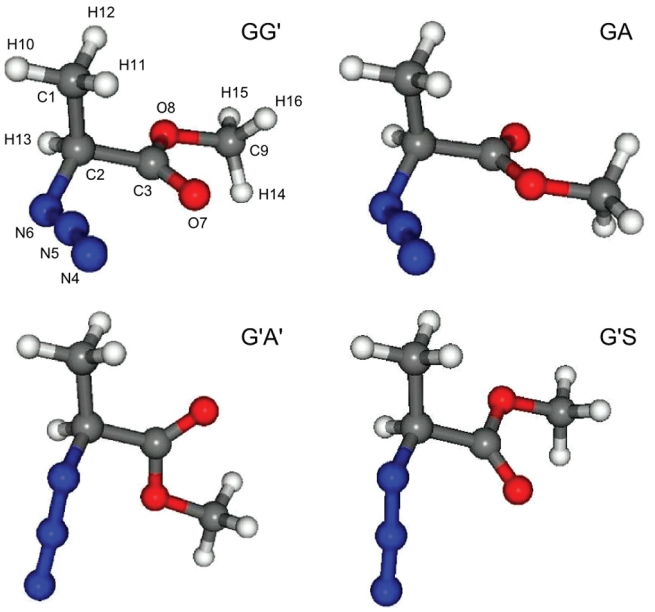

Figure 1. Four lowest-energy conformations of M2AP: GG′ (*gauche*−*gauche*), GA (*gauche*−*anticlinal*), G′A′, and G′S (*gauche*−*synperiplanar*).

The second mechanism, Type 2, proposed for the first time by Dyke and co-workers, involves the formation of a cyclic transition state or stable intermediate, which originates from the transfer of a H-atom or an alkyl group from a remote site of the molecule to the electron-deficient N atom (see Scheme 2). The pyrolyses of ethyl azidoacetate[8] (N_3CH_2COOEt) and methyl (N_3COOMe) and ethyl azidoformate[7] (N_3COOEt) were explained on the basis of this mechanism.

In a more recent study, O'Keeffe et al.[9] revisited the thermal decomposition of 2-azidoacetone, previously investigated by Dyke et al.,[10] using flash pyrolysis in combination with molecular beam mass spectrometry. Low residence times (20−30 μs) in the pyrolysis zone and internal cooling of the nascent thermal decomposition fragments due to supersonic jet expansion allowed the authors to find experimental evidence for the occurrence of both Type 1 and Type 2 mechanisms, at different stages of the thermal decomposition process.

The present work describes the study of the electronic structure and thermal decomposition of methyl 2-azidopropionate (M2AP, $N_3CH_3CHCOOCH_3$), using UVPES and matrix isolation IR spectroscopy. These combined techniques have already proven to be excellent tools in the analysis of the gas-phase thermal decomposition of several azides and investigating their decomposition mechanisms.[6−8,10,11] Moreover, the molecular properties of M2AP have already been investigated by us, in a previous theoretical study.[12]

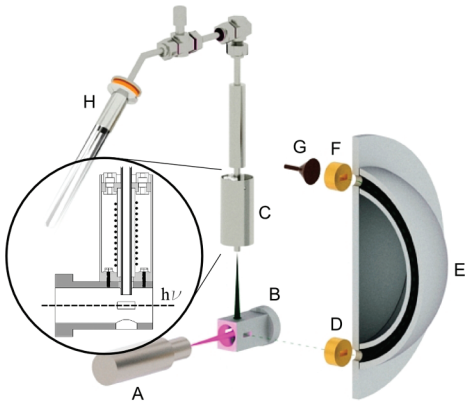

Figure 2. Schematics of the experimental setup, with an expanded view of the resistively heated furnace: A, UV source; B, reaction cell; C, furnace; D, entrance slits; E, energy analyzer; F, exit slits; G, electron detector; and H, liquid sample.

The experimental results presented in this study will be supported and rationalized through computational analysis on (i) the electronic structure and relative populations of the conformers of the parent azide (see Figure 1) and (ii) the possible decomposition pathways and the associated energy barriers for their activation, calculated with high-accuracy ab initio methods.

2. EXPERIMENTAL AND COMPUTATIONAL METHODS

2.1. Sample Preparation and Characterization. Methyl 2-azidopropionate was prepared from the reaction of sodium azide (NaN_3) and methyl 2-bromopropionate ($BrCH_3CHCOOCH_3$). A mixture of $BrCH_3CHCOOCH_3$ and saturated aqueous NaN_3 was stirred continuously, at 60 °C, for 48 h. The product, $N_3CH_3CHCOOCH_3$, was then extracted with dichloromethane (CH_2Cl) and dried over anhydrous Na_2SO_4. Finally, the product was distilled under vacuum, in a Kugelrohr, at 80 °C. The high purity (>99%) of methyl 2-azidopropionate was confirmed in the liquid phase by IR and ^{1}H NMR spectroscopies and in the gas phase by electron impact (EI) mass spectrometry.

The IR spectrum of M2AP exhibited the most intense absorption at 2107 cm^{-1}, assigned to a vibration of the N3 group. Several prominent bands were also present: 2958 cm^{-1} (C−H stretching), 1747 cm^{-1} (C−O stretching), 1454 cm^{-1}, 1257 cm^{-1}, and 1208 cm^{-1}. The 400 MHz ^{1}H NMR spectrum of M2AP in deuterated chloroform ($CDCl_3$) solution revealed three signals: δ = 3.927 (1H, q, J = 7.2 Hz, R_3CH), 3.759 (3H, s, $ROCH_3$), and 1.443 (3H, d, J = 7.2 Hz, RCH_3) ppm. The 100 MHz ^{13}C NMR spectrum of M2AP in deuterated chloroform (CDC_{13}) solution revealed four signals: δ = 171.38 (C═O), 57.23 (R_3CH), 52.56 ($ROCH_3$), and 16.68 (RCH_3) ppm. The 70 eV EI mass spectrum of M2AP showed the parent ion peak at 129 m/z (5%), together with the following fragments: 42 (100%,

dx.doi.org/10.1021/jp2036845 |J. Phys. Chem. A 2011, 115, 8447–8457

C_2H_4N+), 28 (45%, N_2+), 18 (30%, H_2O+), and 59 (28%, $C_2H_3O_2+$) m/z.

Azides are potentially explosive and therefore must be handled with all due precautions. Care was taken to avoid possible explosions at all stages in the preparation and handling of the azide samples. In practice, no explosions were experienced during this work.

2.2. UV Photoelectron Spectroscopy. The UV photoelectron spectrometer used in Lisbon to record the spectra is very similar to the one described elsewhere.[13] An illustrated view of the apparatus is given in Figure 2. It operates under high vacuum conditions, and it consists of a large 150° spherical sector electrostatic analyzer (mean radius = 200 mm) and a DC discharge lamp, capable of producing He(I) (21.22 eV) radiation. Typical working resolution is 30 meV full width at half-maximum (fwhm) as measured for the $(3p)^{-1}\,^2P_{3/2}$ Ar^+ photoelectron line. In a typical experiment, a sample of liquid M2AP is admitted through a PTFE valve, from a glass vial outside the spectrometer reaction chamber, and the vapor passes into the ionization region. The sample was degassed with repeated freeze−pump−thaw cycles prior to its injection into the system.

Before it reaches the ionization region, the M2AP vapor flows through a 45 mm resistively heated stainless-steel furnace (with 4 mm i.d.), where the pyrolysis process takes place (Figure 2, C). The heating resistance is powered by an AC variable transformer which is coupled to a solid state relay (SSR) and a PID controller. The feedback signal is the temperature read at the end of the tube, with a type K (Ni−Cr/Ni−Al) thermocouple. A LabView program drives the PID and sets the oven temperature, which remains stable to within ±1 °C around the desired value. A maximum temperature of ca. 725 °C can be achieved.

The photoelectron spectra of M2AP recorded at room temperature were calibrated by the admission of a small amount of methyl iodide (CH_3I) and argon (Ar) into the reaction chamber.[14] During the thermal decomposition studies, the ionization energy scale calibration was achieved by using the known ionization bands of the major pyrolysis products, such as N_2 and CO, as well as traces of H_2O present in the system.[14]

2.3. Matrix Isolation IR Spectroscopy. The experimental setup for the matrix isolation IR studies, in Southampton, is identical to the one described previously.[11] Briefly, it is based on a conventional closed-cycle cryostat (Air Products, model CSW-202) and an IR grating spectrophotometer (Perkin-Elmer, model 983G), together with a CsI deposition window, maintained at ca. 12 K. The M2AP vapor, precooled in a liquid nitrogen bath, is admitted to the system through a PTFE valve. Prior to its deposition in a N_2 matrix, the M2AP vapor travels through a 150 mm silica furnace (with 5 mm i.d.) which can be resistively heated to 800 °C.

Matrix ratios were estimated to be in excess of 1000:1 (inert gas:sample). Typical deposition times were 40 min at a specific furnace temperature, and the matrix IR spectra were recorded over the 4000−500 cm^{-1} wavenumber range. Similarly to the UVPES experiments, an initial matrix IR spectrum of M2AP was recorded with the heater switched off, to obtain consistent spectra for the parent compound, prior to its thermal decomposition.

2.4. Computational Methods. The optimized geometries of all four lowest-energy conformers of M2AP were taken from our previous work on its molecular properties,[12] obtained with the second-order Møller−Plesset (MP2) perturbation theory[15] and with density functional theory (DFT),[16] using the B3LYP functional. The 6-311++G(d,p) Pople basis set[17] was used in conjunction with the aforementioned methods.

The framework of our computational studies on the valence ionization region is based on the one-electron propagator description[18] (EPT) of the molecular system, implemented at the level of outer-valence Green's function (OVGF) and partial third-order (P3) schemes.[19,20] These methods have already proven to be an invaluable tool in the study of photoelectron spectra of several molecules,[21−23] provided one-electron ionization is valid.

Relative energies of all four M2AP conformers (GG′, GA, G′A′, and GS′) were calculated with the hybrid G3 method.[24] The G3 method provides a computationally economic way of obtaining very accurate relative energies, which include allowance for thermal enthalpy and the zero-point energy (ZPE) corrections. However, the error arising from basis-set superposition (BSSE) is not considered. Estimates for the relative populations of the conformers, at room temperature, were obtained using the Boltzmann distribution formula

$$n_i = \frac{e^{-G_i/kT}}{\sum_n e^{-G_n/kT}} \quad (1)$$

where n_i is the population of the ith conformer; G_i is the Gibbs energy of the ith conformer; and T is the desired temperature. The resulting populations are designated by Boltzmann population ratios (BPRs).

For each conformer, the computed VIEs obtained from the EPT methods were convoluted with Lorentzian functions of 0.4 eV fwhm[25] and summed over to generate the corresponding simulated photoelectron spectrum. This value was chosen to accommodate the broadening due to the vibrational envelope associated with each transition and due to the experimental resolution of the apparatus. The final simulated photoelectron spectrum of M2AP resulted from the sum of each conformer's photoelectron spectrum, weighted by its specific BPR. The same approach was used to produce the simulated IR spectrum of M2AP, which also includes the contribution of all four conformers. The wavenumbers were scaled[26] by 0.9679, and the vibrational lines were convoluted with Lorentzian functions of 10 cm^{-1} fwhm (which was found to give a good fit to the experimental data).

Regarding thermal decomposition pathways, we have carried out several calculations, based on a simple four-step procedure: (i) a relaxed potential energy surface scan along the bond of interest, to detect a possible TS; (ii) full optimization and validation of the candidate TS; (iii) a IRC calculation starting from this TS, connecting reactant, TS, and products; and finally, (iv) the full optimization of the final products. Steps (i) and (iii) were calculated at the B3LYP/6-31+G(d) level, and steps (ii) and (iv) were carried out with the G3 method. All calculations presented in this work were carried out using the Gaussian 09 software.[27]

3. RESULTS AND DISCUSSION

3.1. Electronic Structure and Vibrational Analysis of M2AP. The electronic structure of M2AP was investigated using UVPES and molecular orbital (MO) calculations. None of the M2AP conformations (see Figure 1) studied in this work are of higher symmetry than C_1.

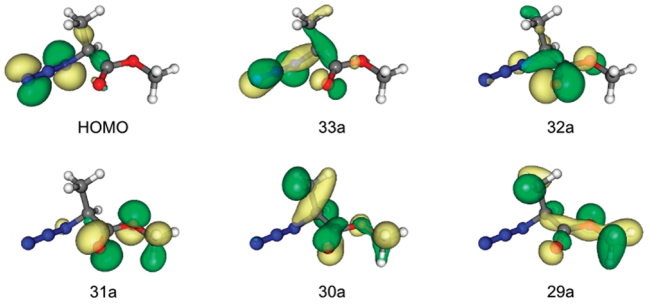

Figure 3. Molecular orbital contours (isovalue = 0.05) of the GG′ conformer of M2AP, from MP2/6-311++G(d,p) results.

Table 1. Calculated Vertical Ionization Energies (VIEs, in eV) of the GG′, G′A′, G′S, and GA Conformers of M2AP, Obtained with the OVGF B Method and the 6-311++G(d,p) Basis, On Optimized MP2/6-311++G(d,p) Geometries

MO	GG′	G′A′	G′S	GA
HOMO	9.20	9.30	9.30	9.25
33a	10.67	10.95	10.78	10.75
32a	11.42	11.64	11.28	11.56
31a	11.70	11.52	11.74	11.62
30a	13.42	13.39	13.31	13.46
29a	13.51	13.55	13.37	13.51
28a	14.03	13.82	14.11	13.95
27a	14.59	14.09	14.26	14.65
26a	14.72	14.26	14.56	14.83
25a	15.34	15.46	15.33	15.29
24a	15.53	16.26	15.92	15.58
23a	16.01	16.17	15.67	16.25
22a	16.56	15.78	16.49	16.45
21a	16.64	16.55	16.61	16.40

The highest occupied molecular orbital (HOMO) and the next five highest HOMOs (33a−29a) of the most stable conformer, GG′, are shown in Figure 3. The first four MOs are almost exclusively comprised of $-N_3$ and $-COOCH_3$ contributions. The HOMO is a $\pi^*_{N_3}$ MO almost entirely localized in the nitrogen group, whereas MO 33a is a $\sigma^*_{N_3}$ from the N_3 moiety, together with a very small contribution from the O7 oxygen lone pair (n_o). Regarding MO 33a, we have used the same σ notation as employed by Bock and Dammel,[4] even though this MO is composed of a rotated p_z orbital between N4−N5 and a rotated antibonding π orbital from N6, relative to the quasi-linear N_3 chain.

The next MO (32a) is localized on the carbonyl lone pair (n_o), in-plane with the $-COOCH_3$ group. MO 31a is a bonding π_{CO} with a considerable amount of antibonding character from the p lone pair (LP) localized on the O8 oxygen. The last MOs appearing in Figure 3, 30a and 29a, result from a combination of different amounts of σ and π orbitals on the $-CH_3(CH)$-$COOCH_3$ moiety: 30a draws its character mainly from a bonding π_{CO}, and 29a features a C−C−O−C σ bonding orbital.

The valence electronic structure of M2AP can be described as a combination of the two outermost occupied orbitals of methyl azide (CH_3N_3) and the two outermost orbitals of methyl formate (MF, $C_2H_4O_2$). The HOMO and MO 33a of M2AP resemble the 3a″ and 12a′ MOs of CH_3N_3, respectively.[4] Analysis of recent work on the occupied MOs of MF[28] clearly shows the similarity between MOs 32a and 31a of M2AP and the MOs 13a′ and 3a″ of MF.

Table 2. Relative Energies (ΔG, kJ/mol) Calculated with the G3 Method (See Text for Details) and Boltzmann Population Ratios (BPR, %) of the GG′, G′A′, GA, and G′S Confomers of M2AP

conformer	ΔG	BPR
GG′	0	34.2
G′A′	0.77	25.0
GA	0.81	24.6
G′S	1.86	16.2

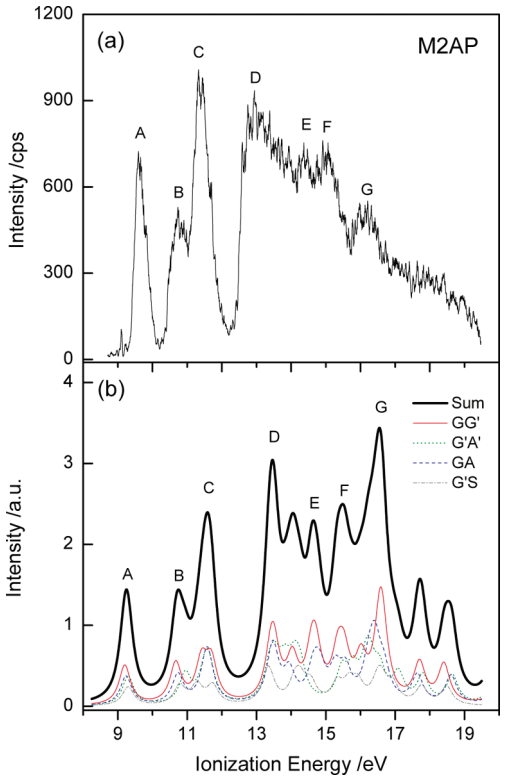

Figure 4. He(I) photoelectron spectrum of M2AP, recorded at room temperature (a), and simulated outer-valence photoelectron spectrum, based on OVGF/6-311++G(d,p) results (b).

The vertical ionization energies (VIEs) of all four conformers, obtained from OVGF/6-311++G(d,p) calculations, are collected in Table 1. Pole strengths associated with all the VIEs calculated with the EPT methods fall between 0.85 and 0.91. The relative populations of the conformers, from G3 results, are estimated at room temperature to be ca. 34, 25, 25, and 16% of GG′, G′A′, GA, and G′S, respectively (see Table 2).

A typical photoelectron spectrum of M2AP, obtained at room temperature, is presented in Figure 4, panel (a), where the bands are labeled A−G. The simulated outer-valence photoelectron spectrum presented in panel (b) of Figure 4 results from the sum of each conformer contribution to the 8−19 eV IE (ionization energy) region of M2AP. The experimental VIEs (vertical ionization energies) of bands A−G, the respective energy

dx.doi.org/10.1021/jp2036845 |J. Phys. Chem. A 2011, 115, 8447–8457

Table 3. Experimental and Calculated Vertical Ionization Energies (VIEs, eV) for M2AP[a]

band	MO	VIE	calcd[b]	character
A	HOMO	9.60 ± 0.03	9.20	$\pi^*_{N_3}$
B	33a	10.74 ± 0.03	10.67	$\sigma^*_{N_3}$
C	32a	11.41 ± 0.04	11.42	n_o
	31a		11.70	π_{co}
D	30a	12.97 ± 0.06	13.42	π_{co}
	29a		13.51	σ
-	28a		14.03	π_{co}
E	27a	14.30 ± 0.07	14.59	π_{co}
	26a		14.72	π_{NN}
F	25a	15.05 ± 0.06	15.34	σ
	24a		15.53	n_N
-	23a		16.01	n_N
G	22a	16.16 ± 0.09	16.56	π_{N_3}
	21a		16.57	π
	20a		16.64	π

[a] MO stands for molecular orbital. [b] From OVGF B results on the GG′ confomer of M2AP.

uncertainties, and the OVGF B orbital energies (GG′ conformer) of M2AP are collected in Table 3, together with the main character of the MO from which ionization occurs for each band.

Although the simulated spectrum of the GG′ conformer alone (the lowest-energy conformer) could be fitted to the experimental spectrum, there are some features that are only explained by the inclusion of the contributions of the other conformers: the right shoulder of peak A, the asymmetric shape of peak B, and the broadening of peak C. The other two most abundant conformers, GA and G′A′, which are almost degenerate (ΔG_{G3} = 0.04 kJ/mol), have similar spectral patterns, but only the GA conformer seems to fit more extensively the experimental spectral band shape, especially the correct profile of bands E and F. The rich 13−17 eV IE region presents several bands, which overlap to form the intricate profile shown in the experimental photoelectron spectrum; the less accurate computational description in this region is mainly due to the fact that, within the OVGF and P3 approximations, "hot bands" and shakeup states are completely neglected. Also, experimentally there is a loss of transmission of the analyzer at low electron kinetic energies (<4 eV) which will reduce the relative intensity of band G and further bands.

However, there is a good agreement between the experimental and the predicted spectra: comparison between the experimental and predicted VIEs in Table 2 and Table 3 (considering only bands A−D and the GG′ conformer of M2AP) leads to mean absolute differences (MADs) of 0.23 and 0.22 eV, from OVGF B and P3 calculations, respectively. For the HF/6-311++G(d,p) orbital energies (scaled by a 0.92 factor) from our previous computational work,[12] the corresponding MAD increases slightly, up to 0.27 eV. On the other hand, unscaled HF orbital energies lead to a very high MAD of 1.25 eV, indicating that the EPT framework is the approximation of choice in terms of predicting VIEs and spectral band profiles.

Figure 5 shows the IR spectrum of M2AP (panel (a)) isolated in the N_2 matrix (12 K), together with the calculated IR spectrum of M2AP (panel (b)), which includes the contributions from the four conformers. Selected vibrational modes are displayed in Table 4, together with their descriptions and the calculated

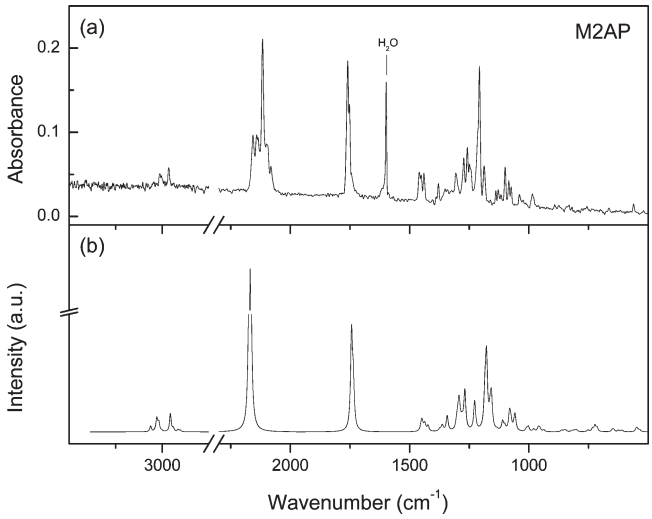

Figure 5. N_2 matrix IR spectrum (3500−500 cm^{-1} spectral range) of M2AP (a) and simulated IR spectrum, based on scaled B3LYP/6-311++G(d,p) results (b).

Table 4. Observed IR Bands of M2AP Isolated in a N_2 Matrix (12 K) and Corresponding Calculated Wavenumbers (cm^{-1}) and Intensities (km mol^{-1})[a]

mode	assign.	calcd[b] wavenumber	observed wavenumber	calcd[b] intensity
ν_{35}	ν(N_3)as	2168	2117	511
ν_{34}	ν(C═O)	1743	1760/1752	177
ν_{24}	w(CH_3)	1177	1207	222
ν_{23}	w(CH_3)	1157	1187	159

[a] ν, stretching. w, wagging. δ, bending. as, asymmetric. [b] Scaled B3LYP/6-311++G(d,p) calculations on the GG′ conformer (see text for details).

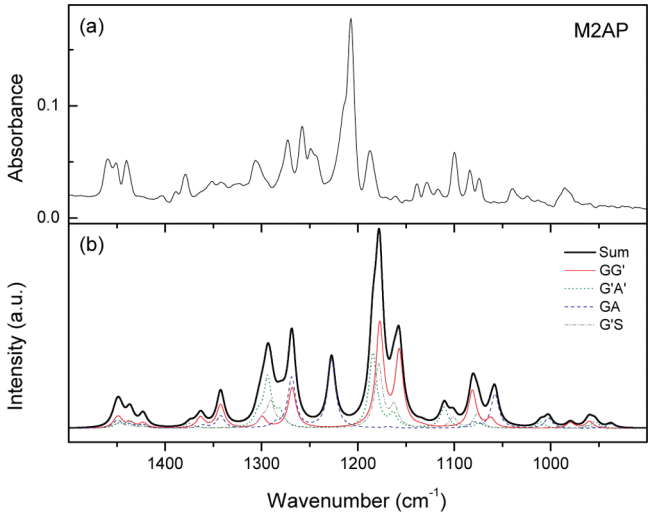

Figure 6. N_2 matrix IR spectrum (1500−900 cm^{-1} spectral range) of M2AP (a) and simulated IR spectrum, based on scaled B3LYP/6-311++G(d,p) results (b).

(from B3LYP/6-311++G(d,p) scaled wavenumbers of the GG′ conformer) and observed wavenumbers. The easily identifiable

dx.doi.org/10.1021/jp2036845 |J. Phys. Chem. A 2011, 115, 8447–8457

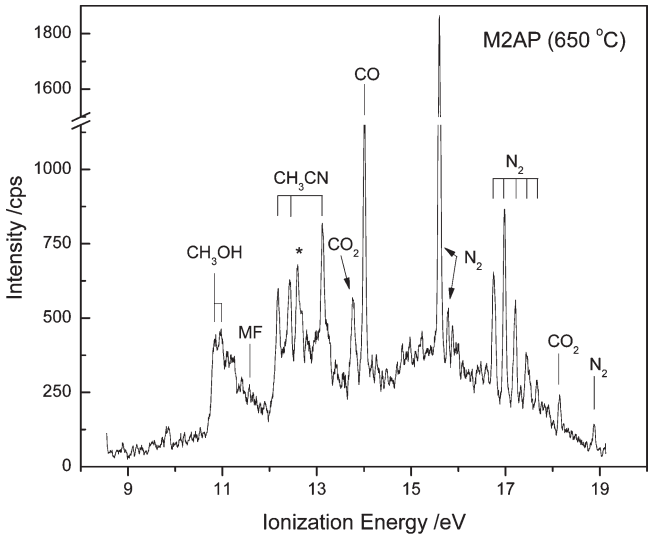

Figure 7. He(I) photoelectron spectrum of the thermal decomposition of M2AP, taken at 650 °C. The asterisk marks the characteristic ionization line of H_2O.

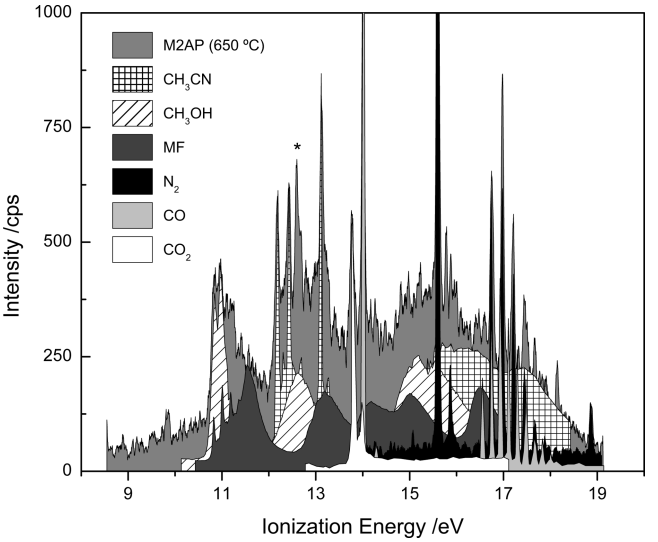

Figure 8. Detail of the He(I) photoelectron spectrum of the thermal decomposition of M2AP (gray), taken at 650 °C, with estimated contributions from the decomposition species CH_3CN (cross-hatched), CH_3OH (hatched), MF (dark gray), N_2 (black), CO (light gray), and CO_2 (white). The asterisk marks the characteristic ionization line of H_2O.

modes are useful to monitor the thermal decomposition evolution of M2AP, in the matrix IR studies.

In Figure 6, the region between 1500 and 900 cm^{-1} is presented in more detail, with the denoted contributions of each conformer. Apart from a slightly shifted main peak ($w(CH_3)$, 1207 cm^{-1} obsd, 1177 cm^{-1} calcd), toward the low wavenumbers region, the computed spectrum shows a very good agreement with the experimental matrix IR results. The marked presence of the other conformers, confirmed by the three consecutive peaks, immediately at the left-hand side of the most intense peak, is quite interesting. The absorption line at 1249 cm^{-1} ($w(CH_3)$, 1227 cm^{-1} calcd) is only due to the GA conformer, whereas the band at 1273 cm^{-1} (δ(N−C−H), 1293 cm^{-1} calcd) comes essentially from the G′A′ conformer.

3.2. Thermal Decomposition of M2AP: UVPES Studies. Several spectra were obtained at different stages of the pyrolysis process, from room temperature to approximately 650 °C. A typical full thermal decomposition spectrum of M2AP, taken at 650 °C, is shown in Figure 7, where clear signals of nitrogen (N_2, VIE = 15.60 eV), acetonitrile (CH_3CN, VIE = 12.21 eV), methanol (CH_3OH, VIE = 10.95 eV), carbon monoxide (CO, VIE = 14.01 eV), and dioxide (CO_2, VIE = 13.78 eV) can be identified. Methyl formate (MF, $HCOOCH_3$) is also detectable as a broad shoulder at the right side of the first band of methanol. The first and second bands of MF, at 10.99 and 11.54 eV (VIEs), respectively, are thus overlapped with the first band of CH_3OH, which hinders its clear identification in the spectrum.

The thermal decomposition of M2AP starts at ca. 400 °C, when the intensity of band A of the parent azide (at 9.60 eV) diminishes and the valley between bands B and C disappears. This is accompanied by the elimination of N_2, almost simultaneous to the appearance of CO and CO_2 in the spectrum. The transformation occurring in the IE range of bands B/C of M2AP is due to the formation of methanol, with an intense first band centered at 10.95 eV. Subtraction of a properly normalized room temperature spectrum of M2AP from the pyrolysis spectra obtained at the early stages of decomposition (400−500 °C) revealed the clear presence of CH_3OH and also the contribution of MF, overlapped in the 10.0−12.5 eV IE range. CH_3CN is also

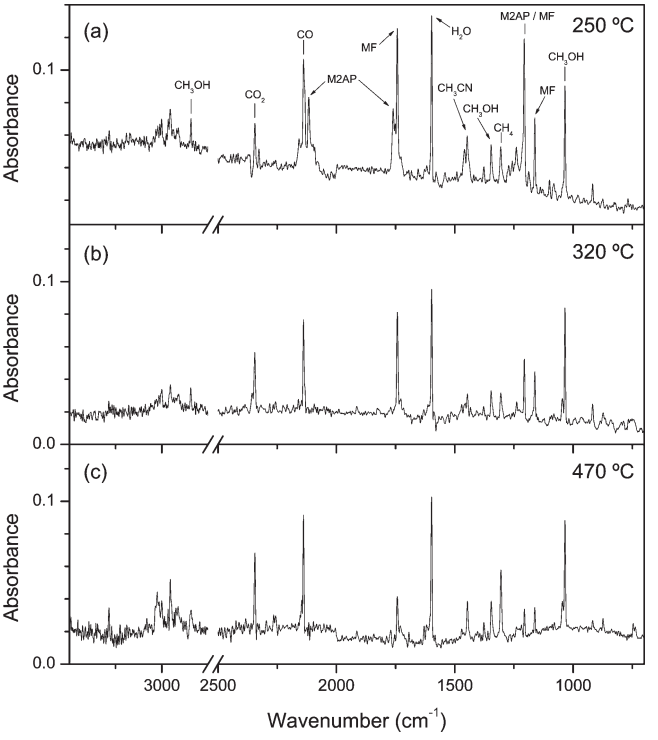

Figure 9. N_2 matrix IR spectrum (3500−700 cm^{-1} spectral range) of M2AP after partial pyrolysis at 250 °C (a) and 320 °C (b) and after complete pyrolysis at 470 °C (c).

formed in this first stage of decomposition, with the increase of its three very distinctive bands (12.21, 12.47, and 13.16 eV) in the 12.0−13.5 eV IE region. The individual contributions of each thermal decomposition product to the overall spectral band shape (at 650 °C) can best be seen in Figure 8.

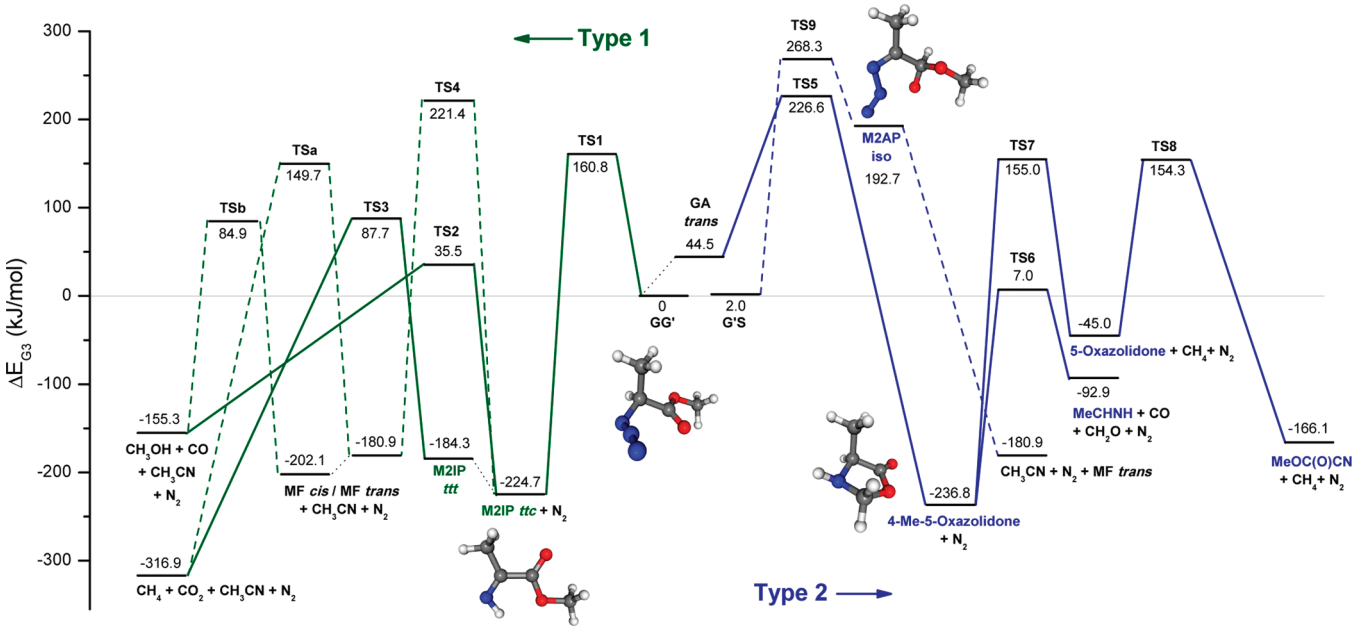

Figure 10. Potential energy diagram (in kJ/mol) for the thermal decomposition of M2AP, calculated with the G3 method. Pathways derived from a Type 1 mechanism are shown at the left-hand side, and pathways derived from a Type 2 mechanism are shown at the right-hand side of the diagram. The G3 energy barriers associated with the decomposition of MF (left side) were taken from the work of Metcalfe et al.[30] All other results are from this study.

From 500 to 650 °C, there were no observed changes in the pyrolysis process, with an expected increase in the intensity of all the decomposition products with increased temperature. At 650 °C, the first band of M2AP has completely disappeared, indicating full decomposition of this molecule.

3.3. Thermal Decomposition of M2AP: Matrix Isolation IR Studies. After obtaining the matrix IR spectrum of M2AP at room temperature, the heater was switched on, and the temperature slowly increased, until almost full decomposition was observed. At each step, the matrix IR spectra were obtained after 40 min of deposition, during which the temperature was held constant. The results are shown in Figure 9, where the spectral evolution at different stages of the thermal decomposition can be seen. It should be noted that the temperatures at which partial and full decomposition were observed are lower than the corresponding temperatures in the UVPES study as the pressures and pumping speeds were different from those used in the UVPES study.

The IR studies reveal that the M2AP molecule starts to decompose around 250 °C, with the simultaneous appearance of the characteristic absorption peaks of CO (2139 cm^{-1}), CO_2 (2347 cm^{-1}), CH_3OH (1034, 1347, 2842 cm^{-1}), CH_3CN (1447, 1378 cm^{-1}), and methyl formate (MF, at 1743, 1207, 1162, 918 cm^{-1}). Methane (CH_4), clearly identifiable by the 1306 cm^{-1} band, also appears as a product, in the early stages of the thermal decomposition. This represents extra information from the matrix studies compared to those obtained from the UVPES results because the photoelectron band of CH_4 is very broad and has a very low cross-section, in the He(I) IE range of the photoelectron spectra.

Careful comparison between the IR spectra obtained at 320 and 470 °C reveals an interesting feature: in this temperature range, the absorption bands assigned to MF decrease significantly, whereas the bands from the other products remain at approximately the same height. MF can indeed decompose into CH_4 and CO_2, but that pathway is not the lowest-energy pathway: MF decomposition yields predominantly methanol and CO.[29] This suggests that two channels, at least, are leading to the formation of methanol and that the one involving methyl formate and its decomposition is not the most favorable pathway.

3.4. Mechanism of Gas-Phase Thermal Decomposition of M2AP. The thermal decomposition studies with both the matrix IR and the UVPES techniques show that N_2, CO, CH_3CN, CH_3OH, MF, CO_2, and CH_4 are being formed from the pyrolysis of M2AP. However, only in the matrix IR spectra is CH_4 clearly identifiable. In addition, the UVPES spectra suggest that N_2 appears almost simultaneously with the other decomposition products, namely, CO, CH_3OH, and CH_3CN, pointing to the occurrence of a multifragmentation mechanism.

Although no clear evidence for the formation of an imine or an unknown intermediate has been detected experimentally, our computational studies on the thermal decomposition of M2AP have focused primarily on the two known mechanisms: a Type 1 mechanism, associated with the imine formation, and a Type 2 mechanism, associated with the formation of a cyclic TS/intermediate. These results are summarized in the potential energy diagram for the thermal decomposition of M2AP, presented in Figure 10. All the transition structures are depicted in Figure 11.

3.4.1. Imine Formation through a 1,2-H Shift Synchronous with N_2 Elimination (a Type 1 Mechanism). Studies concerning the Type 1 mechanism, i.e., imine (R′RC═NH) formation with N_2 elimination, revealed the formation of methyl 2-iminopropionate (M2IP) from the GG′ conformer of M2AP, through a 160.8 kJ/mol energy barrier (ΔE_{G3}). Elimination of N_2 from the azide chain is assisted by the H-atom transfer (H13) to the nitrogen atom (N6), in a synchronous process, through the formation of TS1 (Figure 10, left side).

The M2IP molecule can adopt a number of conformations, which are essentially distinguished by the values of three dihedral angles: C1−C2−N6−H, C1−C2−C3−O8, and C9−O8−C3−O7 (where the atom labeling is the same as that used in

dx.doi.org/10.1021/jp2036845 |J. Phys. Chem. A 2011, 115, 8447–8457

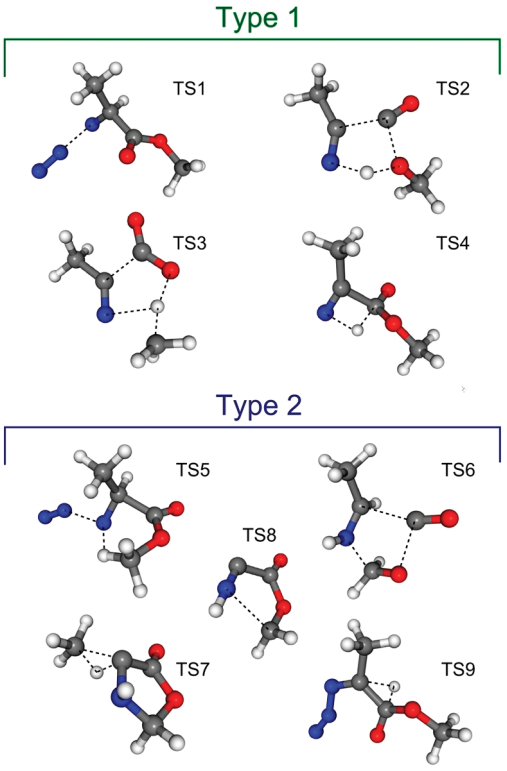

Figure 11. Geometry of all the transition structures, calculated with the G3 method, involved in the thermal decomposition of M2AP, originated by either a Type 1 or a Type 2 mechanism.

Figure 1). The first angle sets the position of the imine H-atom relative to the central CH_3 group; the second angle sets the position of the HN═C−CH_3 fragment relative to the MF group; and finally, the third angle distinguishes between the $\mathbb{E}$ and $\mathbb{Z}$ geometries of the $COOCH_3$ group. The M2IP structure shown in Figure 10 is thus denoted as *trans*−*trans*−*cis* (*ttc*). All other conformers of M2IP are named according to the above scheme.

Calculations on the *ttc* conformer of M2IP show that it can dissociate into CO, CH_3OH, and CH_3CN, by a simple H-atom transfer (H13) to the oxygen atom (O8). The activation barrier involved in this process is calculated at 260.2 kJ/mol, obtained from the difference between the G3 energies of M2IP *ttc* and the transition structure TS2. One of the conformers of M2IP has the CH_3 groups in opposite directions and the MF moiety in a *trans* ($\mathbb{E}$) configuration. This M2IP *ttt* conformer is 40.4 kJ/mol above the *ttc* conformer and can break into CH_4, CO_2, and CH_3CN, with an activation energy of 272.0 kJ/mol, through the transition structure TS3.

It is appropriate to investigate if MF can be formed also from M2IP *ttc*, in a fragmentation process which gives rise to CH_3CN + MF. Energy-wise, the lowest-energy path for this to be accomplished is by letting the H13 hydrogen move to the vicinity of the carbon atom (see Figure 11, TS4). The high-energy barrier (ΔE_{G3} = 446.1 kJ/mol) clearly indicates that this process is very unlikely to compete with the former routes, although it accounts for MF formation.

The decomposition of MF was recently analyzed in a study by Metcalfe et al.,[30] in which the author concluded that MF's decomposition was dominated by a single channel producing CH_3OH + CO and that the other two decomposition channels yielding CH_2O + CH_2O and CH_4 + CO_2, respectively, could be removed from the kinetic mechanism describing the pyrolysis of MF. The G3 energy differences between MF and the transitions structures leading to CH_3OH + CO and CH_4 + CO_2, calculated by Metcalfe et al.[30] with the G3 method, are included in Figure 10, for comparison.

Overall, the Type 1 mechanism can be applied to the thermal decomposition of M2AP, effectively leading to the formation of N_2 and an imine (M2IP *ttc*), from which CH_3OH, CO, and CH_3NH can be formed, through accessible energy barriers. MF formation from this imine requires a large amount of energy to occur, and even then, CH_4 and CO_2 do not originate from the most probable decomposition route of MF.[29,30] On the other hand, the M2IP imine can alternatively adopt a *ttt* conformation and decompose to give CH_4 + CO_2 + CH_3CN, through a lower barrier (272.0 kJ/mol) than the one required for MF to decompose into CH_4 + CO_2 (330.6 kJ/mol). These results can be summarized as follows

$$N_3CH(CH_3)CO_2CH_3 \xrightarrow{TS1} HN{=}C(CH_3)CO_2CH_3 + N_2 \quad (2)$$

$$HN{=}C(CH_3)CO_2CH_3 \xrightarrow{TS2} CO + CH_3OH + CH_3CN \quad (3)$$

$$HN{=}C(CH_3)CO_2CH_3 \xrightarrow{TS3} CO_2 + CH_4 + CH_3CN \quad (4)$$

$$HN{=}C(CH_3)CO_2CH_3 \xrightarrow{TS4} HC(O)OCH_3 + CH_3CN \quad (5)$$

$$HC(O)OCH_3 \xrightarrow{TSa} CO_2 + CH_4 \quad (6)$$

$$HC(O)OCH_3 \xrightarrow{TSb} CO + CH_3OH \quad (7)$$

3.4.2. Heterocyclic Formation Synchronous with N_2 Elimination (A Type 2 Mechanism). If the 1,2-R rearrangement (R being a hydrogen or alkyl group) is initiated from a remote site of the molecule, a cyclic intermediate may be formed, either as a five-membered TS or as a more stable ring structure. Likely donors in this process are the methyl hydrogens closest to the electron-deficient N in M2AP. However, in the case of the CH_3 group associated with the MF moiety, this implies some prior conformational rearrangement in M2AP into a more favorable geometry, one in which the −$COOCH_3$ group assumes a *trans* configuration. Hence, the optimized structures of a set of M2AP conformers, lying 35−45 kJ/mol above the GG′ conformation, were computed with the G3 method, and possible hydrogen transfers from remote alkyl sites were considered.

From the *trans* configuration of M2AP G′A′, a five-membered heterocyclic compound—4-methyl-1,3-oxazolidine-5-one—was found to be formed through migration of the methyl hydrogen onto the nitrogen atom, simultaneous to the N_2 elimination (TS5, Figure 10), with an activation energy of 182.1 kJ/mol (relative to M2AP G′A′ *trans*). The nonmethylated form of this five-membered intermediate has been already identified in a previous study by Dyke et al.,[7] of the pyrolysis of ethyl azidoformate ($N_3COO(CH_2)CH_3$). At that time, it was proposed on the basis of results of ab initio calculations that the oxazolidone could

further decompose into CO_2 and Me(CH)NH (ethanimine). Applying the same reasoning to the decomposition of 4-Me-5-oxazolidone, a transition structure (TS6) leading to the production of ethanimine was found to be formed from three interdependent steps: breaking of the C−C bond, release of CO, and formation of formaldehyde (CH_2O). The proposed computed reaction, shown in the lower right side of Figure 10, has an activation energy of 243.8 kJ/mol and gives MeCHNH, CO, and CH_2O from 4-Me-5-oxazolidone.

Although CO is observed as a decomposition product, the easily identifiable CH_2O is not. Ethanimine is the resulting imine from the pyrolysis of ethyl azide,[4] and it can decompose via two competitive[31] routes: CH_4 + HNC and H2 + CH_3CN. Again, although CH_3CN is found within the thermal decomposition products detected spectroscopically, no evidence of HNC or HCN was found. Therefore, in spite of being energetically feasible, no support for the decomposition route involving formation of ethanimine from 5-oxazolidone was obtained experimentally.

Another way for the 4-Me-5-oxazolidone to decompose is through a 1,2-H shift onto the methyl substituent, which implies a high activation energy of 391.8 kJ/mol (TS7) and leaves behind CH_4 + 5-oxazolidone as products. The 5-oxazolidone can then undergo ring opening and isomerize into methyl cyanoformate (MeOC(O)CN), through a 199.3 kJ/mol energy barrier (TS8). Previous work on the pyrolysis of cyanoformates by Sheppard[32] showed that MeOC(O)CN loses CO_2 and forms CH_3CN (at 700 °C), two of the decomposition products detected in our UVPES results.

An alternative, simple mechanism, which fits the Type 2 format because it does not imply a nitrene or an imine, leads to the formation of an M2AP isomer and is shown in the upper right side of Figure 10. This isomer is easily formed from the GS′ conformer of M2AP, through a 1,2-H shift of the H13 atom onto the C3 atom, which needs 266.3 kJ/mol to be activated. This isomer then dissociates with no barrier into CH_3CN, N_2, and MF. The former route represents the only Type 2 based explanation for the formation of MF and is energetically more favorable (ΔE_{G3} = 266.3 kJ/mol) than the equivalent Type 1 reaction (M2AP GG′ → M2IP *ttc* → MF, max. ΔE_{G3} = 446.1 kJ/mol).

A Type 2 mechanism could in fact be used to explain the presence of the products in the experimental spectra. However, the 5-oxazolidone intermediate or its methylated form were not detected experimentally, whereas in related studies on ethyl azidoformate, formation of the oxazolidone intermediate was spectroscopically verified by UVPES and matrix isolation IR.[7] If the formation of the M2AP isomer is included in the Type 2 description, then it fulfills the need for explaining the presence of MF, something which we were not able to model (computationally) from the decomposition of the oxazolidone. These two compounds, 4-Me-5-oxazolidone and the M2AP isomer, are thus needed if one wishes to explain the complete thermal decomposition of M2AP, without the formation of an imine or nitrene. The proposed routes involving 4-Me-5-oxazolidone and M2AP are summarized as follows

$$N_3CH(CH_3)CO_2CH_3 \xrightarrow{TS5} \text{4-Me-5-oxazolidone} + N_2 \quad (8)$$

$$\text{4-Me-5-oxazolidone} \xrightarrow{TS6} CH_3(CH)NH + CO + CH_2O \quad (9)$$

$$CH_3(CH)NH \rightarrow CH_4 + HNC \quad (10)$$

$$CH_3(CH)NH \rightarrow H_2 + CH_3CN \quad (11)$$

$$\text{4-Me-5-oxazolidone} \xrightarrow{TS7} \text{5-oxazolidone} + CH_4 \quad (12)$$

$$\text{5-oxazolidone} \xrightarrow{TS8} CH_3OC(O)CN \quad (13)$$

$$CH_3OC(O)CN \rightarrow CO_2 + CH_3CN \quad (14)$$

$$N_3CH(CH_3)CO_2CH_3 \xrightarrow{TS9} \text{M2AP isomer} \quad (15)$$

$$\text{M2AP isomer} \rightarrow HC(O)OCH_3 + CH_3CN + N_2 \quad (16)$$

Overall, considering the analysis just in terms of the activation barriers, the thermal decomposition of M2AP is clearly dominated by the Type 1 mechanism. Relative to the most abundant conformer, M2AP GG′, the initial formation of the imine is 65.8 kJ/mol less expensive than the formation of 4-Me-5-oxazolidone and requires 107.5 kJ/mol less energy to activate than the route leading to the M2AP isomer. The Type 2 mechanism can only be considered energetically more advantageous over Type 1 in a latter stage of the pyrolysis, in which the MF formation from the M2AP isomer clearly requires less energy than the one needed in the dissociation of M2IP into MF and CH_3CN. Also, the experimental evidence from UVPES and IR matrix isolation spectroscopy favors a Type 1 mechanism as the dominant mechanism.

4. CONCLUSION

Methyl 2-azidopropionate (M2AP) has been synthesized and characterized by means of ^{1}H NMR and IR spectroscopies, mass spectrometry, and photoelectron spectroscopy. Results from IR absorption and UVPES were interpreted with the aid of molecular orbital calculations. The valence photoelectron spectrum of M2AP encompasses contributions from the four lowest-energy conformations (GG′, GA, G′A′, and G′S) and consists of seven bands in the 8.0−17.0 eV IE region. Its HOMO VIE is 9.60 ± 0.03 eV, which corresponds to the ionization of a π^* MO located in the azide chain. The next two uppermost MOs are essentially nonbonding orbitals. A $(\sigma^*_{N_3})^{-1}$ ionization occurs at 10.74 ± 0.03 eV, and an oxygen 2p lone-pair $(n_o)^{-1}$ ionization occurs at 11.41 ± 0.04 eV. Comparison between the experimental matrix IR spectrum of M2AP and the simulated spectrum based on DFT calculations, at room temperature, also points to the coexistence of all four lowest-energy conformers.

The thermal decomposition of M2AP in the gas phase was also studied by UVPES and matrix isolation IR spectroscopy. For this purpose, a new and more stable heating system was developed and successfully coupled to a photoelectron spectrometer. The experimental studies revealed N_2, CH_3OH, CH_3CN, CH_4, CO, CO_2, and methyl formate (MF) as the final decomposition products. Unfortunately, no intermediate species were detected spectroscopically.

Two already established mechanisms of decomposition, Type 1 (imine/nitrene formation) and Type 2 (heterocyclic formation), were used to understand the pyrolysis process of M2AP. Computational studies of two mechanisms, based on

results from the G3 hybrid method, revealed the predominance of the Type 1 option over Type 2.

The proposed Type 1 pathways imply the formation of methyl 2-iminopropionate (M2IP) synchronous with the N_2 elimination, through a 160.8 kJ/mol barrier, and further decomposition of M2IP via two competitive routes: one accounting for CO, CH_3OH, and CH_3CN (ΔE_{G3} = 260.2 kJ/mol) and another leading to CO_2, CH_4, and CH_3CN (ΔE_{G3} = 268.6 kJ/mol). Type 2 pathways involve the formation of a cyclic intermediate, 4-Me-5-oxazolidone, together with the N_2 elimination (ΔE_{G3} = 182.1 kJ/mol), which could compete with the imine formation. On the other hand, some easily detectable products which follow from the decomposition of oxazolidone (CH_2O and HCN from the decomposition of ethanimine) were not observed experimentally. Also, we were unable to propose a plausible reaction which accounted for the formation of CH_3OH, a major pyrolysis product, from the oxazolidone intermediate. The former two arguments are sufficient to disfavor a Type 2 mechanism over a Type 1 mechanism.

Finally, an isomer of M2AP was found to be formed from a 1, 2-H shift to a central carbon atom (ΔE_{G3} = 268.3 kJ/mol), which dissociates without any barrier to form CH_3CN, N_2, and MF. As MF can decompose into CH_3OH + CO and CH_4 + CO_2, through 287.0 and 330.6 kJ/mol energy barriers, respectively, then this "Type 3" mechanism also accounts for all the detected decomposition products. Although not capable of competing with the Type 1 and 2 mechanisms, in terms of overall activation energy, further experimental and computational work is needed to clarify its existence.

In summary, a Type 1 mechanism accounts for the observed pyrolysis behavior and all the observed products and is the dominant decomposition mechanism of M2AP.

■ ASSOCIATED CONTENT

Supporting Information. Energy-minimized Cartesian coordinates and energies (Table S1) of all compounds under study, calculated at the G3 level of theory. VIEs of the four lowest-energy conformers of M2AP, obtained with the P3 method (Table S2). This material is available free of charge via the Internet at http://pubs.acs.org.

■ AUTHOR INFORMATION

Corresponding Author

*E-mail: ruipinto@fct.unl.pt. Phone: +351 212 948 576. Fax: +351 212 948 549.

Notes

[⊥]Deceased.

■ ACKNOWLEDGMENT

R. M. Pinto would like to acknowledge Fundação para a Ciência e Tecnologia (FCT) for the grant SFRH/BD/40308/2007. The authors would like to thank J. P. Santos for providing computational support. This study is dedicated to our colleague, friend, and coauthor, Dr. Steve Ogden, who sadly passed away just before the end of this work.

■ REFERENCES

(1) Patai, S. *The chemistry of the azido group*; Chemistry of functional groups; Interscience Publishers: New York, 1971.

(2) Bräse, S.; Banert, K. *Organic Azides: Syntheses and Applications*; John Wiley & Sons: New York, 2009.

(3) Bräse, S.; Gil, C.; Knepper, K.; Zimmermann, V. *Angew. Chem., Int. Ed.* **2005**, *44*, 5188–5240.

(4) Bock, H.; Dammel, R. *Angew. Chem., Int. Ed.* **1987**, *26*, 504–526.

(5) Nguyen, M. T.; Sengupta, D.; Ha, T.-K. *J. Phys. Chem.* **1996**, *100*, 6499–6503.

(6) Dyke, J. M.; Levita, G.; Morris, A.; Ogden, J. S.; Dias, A. A.; Algarra, M.; Santos, J. P.; Costa, M. L.; Rodrigues, P.; Barros, M. T. *J. Phys. Chem. A* **2004**, *108*, 5299–5307.

(7) Dyke, J. M.; Levita, G.; Morris, A.; Ogden, J. S.; Dias, A. A.; Algarra, M.; Santos, J. P.; Costa, M. L.; Rodrigues, P.; Andrade, M. M.; Barros, M. T. *Chem.—Eur. J.* **2005**, *11*, 1665–1676.

(8) Hooper, N.; Beeching, L. J.; Dyke, J. M.; Morris, A.; Ogden, J. S.; Dias, A. A.; Costa, M. L.; Barros, M. T.; Cabral, M. H.; Moutinho, A. M. C. *J. Phys. Chem. A* **2002**, *106*, 9968–9975.

(9) O'Keeffe, P.; Scotti, G.; Stranges, D.; Rodrigues, P.; Barros, M. T.; Costa, M. L. *J. Phys. Chem. A* **2008**, *112*, 3086–3093.

(10) Dyke, J. M.; Groves, A. P.; Morris, A.; Ogden, J. S.; Catarino, M. I.; Dias, A. A.; Oliveira, A. M. S.; Costa, M. L.; Barros, M. T.; Cabral, M. H.; Moutinho, A. M. C. *J. Phys. Chem. A* **1999**, *103*, 8239–8245.

(11) Dyke, J. M.; Groves, A. P.; Morris, A.; Ogden, J. S.; Dias, A. A.; Oliveira, A. M. S.; Costa, M. L.; Barros, M. T.; Cabral, M. H.; Moutinho, A. M. C. *J. Am. Chem. Soc.* **1997**, *119*, 6883–6887.

(12) Pinto, R. M.; Dias, A. A.; Costa, M. L. *J. Mol. Struct.: THEOCHEM* **2009**, *894*, 80–87.

(13) Morris, A.; Jonathan, N.; Dyke, J. M.; Francis, P. D.; Keddar, N.; Mills, J. D. *Rev. Sci. Instrum.* **1984**, *55*, 172–181.

(14) Kimura, K. *Handbook of HeI photoelectron spectra of fundamental organic molecules: ionization energies, ab initio assignments, and valence electronic structure for 200 molecules*; Japan Scientific Societies Press; Halsted Press: Tokyo; New York, 1981.

(15) Møller, C.; Plesset, M. S. *Phys. Rev.* **1934**, *46*, 618–622.

(16) Parr, R.; Weitao, Y. *Density-Functional Theory of Atoms and Molecules*; Oxford University Press: New York, 1994.

(17) Krishnan, R.; Binkley, J. S.; Seeger, R.; Pople, J. A. *J. Chem. Phys.* **1980**, *72*, 650–654.

(18) Cederbaum, L. S. *J. Phys. B* **1975**, *8*, 290.

(19) von Niessen, W.; Schirmer, J.; Cederbaum, L. S. *Comput. Phys. Rep.* **1984**, *1*, 57–125.

(20) Ortiz, J. V. *J. Chem. Phys.* **1996**, *104*, 7599–7605.

(21) Zaytseva, I. L.; Trofimov, A. B.; Schirmer, J.; Plekan, O.; Feyer, V.; Richter, R.; Coreno, M.; Prince, K. C. *J. Phys. Chem. A* **2009**, *113*, 15142–15149.

(22) Trofimov, A. B.; Schirmer, J.; Kobychev, V. B.; Potts, A. W.; Holland, D. M. P.; Karlsson, L. *J. Phys. B* **2006**, *39*, 305.

(23) Chrostowska, A.; Nguyen, T. X. M.; Dargelos, A.; Khayar, S.; Graciaa, A.; Guillemin, J. *J. Phys. Chem. A* **2009**, *113*, 2387–2396.

(24) Curtiss, L. A.; Raghavachari, K.; Redfern, P. C.; Rassolov, V.; Pople, J. A. *J. Chem. Phys.* **1998**, *109*, 7764–7776.

(25) Potts, A. W.; Holland, D. M. P.; Trofimov, A. B.; Schirmer, J.; Karlsson, L.; Siegbahn, K. *J. Phys. B* **2003**, *36*, 3129.

(26) Andersson, M. P.; Uvdal, P. *J. Phys. Chem. A* **2005**, *109*, 2937–2941.

(27) Frisch, M. J.; Trucks, G. W.; Schlegel, H. B.; Scuseria, G. E.; Robb, M. A.; Cheeseman, J. R.; Scalmani, G.; Barone, V.; Mennucci, B.; Petersson, G. A.; Nakatsuji, H.; Caricato, M.; Li, X.; Hratchian, H. P.; Izmaylov, A. F.; Bloino, J.; Zheng, G.; Sonnenberg, J. L.; Hada, M.; Ehara, M.; Toyota, K.; Fukuda, R.; Hasegawa, J.; Ishida, M.; Nakajima, T.; Honda, Y.; Kitao, O.; Nakai, H.; Vreven, T.; Montgomery, J. A., Jr.; Peralta, J. E.; Ogliaro, F.; Bearpark, M.; Heyd, J. J.; Brothers, E.; Kudin, K. N.; Staroverov, V. N.; Kobayashi, R.; Normand, J.; Raghavachari, K.; Rendell, A.; Burant, J. C.; Iyengar, S. S.; Tomasi, J.; Cossi, M.; Rega, N.; Millam, J. M.; Klene, M.; Knox, J. E.; Cross, J. B.; Bakken, V.; Adamo, C.; Jaramillo, J.; Gomperts, R.; Stratmann, R. E.; Yazyev, O.; Austin, A. J.; Cammi, R.; Pomelli, C.; Ochterski, J. W.; Martin, R. L.; Morokuma, K.; Zakrzewski, V. G.; Voth, G. A.; Salvador, P.; Dannenberg, J. J.; Dapprich, S.; Daniels, A. D.; Farkas, .; Foresman, J. B.; Ortiz, J. V.; Cioslowski, J.;

Fox, D. J. *Gaussian 09*, revision A.02.; Gaussian Inc.: Wallingford CT, 2009.
(28) Nunes, Y.; Martins, G.; Mason, N. J.; Duflot, D.; Hoffmann, S. V.; Delwiche, J.; Hubin-Franskin, M.-J.; Limão-Vieira, P. *Phys. Chem. Chem. Phys.* **2010**, *12*, 15734–15743.
(29) Francisco, J. S. *J. Am. Chem. Soc.* **2003**, *125*, 10475–10480.
(30) Metcalfe, W. K.; Simmie, J. M.; Curran, H. J. *J. Phys. Chem. A* **2010**, *114*, 5478–5484.
(31) Arenas, J. F.; Marcos, J. I.; López-Tocón, I.; Otero, J. C.; Soto, J. *J. Chem. Phys.* **2000**, *113*, 2282–2289.
(32) Sheppard, W. A. *J. Org. Chem.* **1962**, *27*, 3756–3759.